Journal of The Electrochemical Society

Application of Rod-Like Li_6PS_5Cl Directly Synthesized by a Liquid Phase Process to Sheet-Type Electrodes for All-Solid-State Lithium Batteries

JES Focus Issue of Selected Papers from IMLB 2018

Application of Rod-Like Li_6PS_5Cl Directly Synthesized by a Liquid Phase Process to Sheet-Type Electrodes for All-Solid-State Lithium Batteries

Sunho Choi, Jiu Ann, Jiyae Do, Seungwoo Lim, Chanhwi Park, and Dongwook Shin [z]

Division of Materials Science & Engineering, Hanyang University, Seongdong-gu, Seoul 04763, Korea

All-solid-state lithium batteries employing sulfide-based solid electrolytes have emerged as promising next-generation batteries for large-scale energy storage applications because of their safety and high energy density. Among them, Li_6PS_5X (X = Cl, Br, I) with an argyrodite structure synthesized by planetary milling exhibits a rather high lithium ion conductivity of 10^{-2} – 10^{-3} S cm^{-1} at room temperature. Unfortunately, the planetary milling process has the disadvantage of producing the solid electrolytes with large, round-shaped particles. Recently, the solid electrolytes have been synthesized by not the mechanical milling but the liquid-phase process, which facilitates synthesis of sub-micrometer- to nanometer-sized solid electrolyte particles. It is important to reduce the particle size of the solid electrolyte to promote intimate contact with the active material in the composite cathode. Here, rod-like Li_6PS_5Cl solid electrolyte with a high ionic conductivity of 1.1×10^{-3} S cm^{-1} at room temperature was, for the first time, directly prepared by a liquid phase process using only a stirring method. SEM images showed the electrolyte had a rod-like morphology with a length of 20–30 μm and a width of 2–3 μm. The composite cathode was prepared from a slurry and the cell performances were investigated.

 [DOI: 10.1149/2.0301903jes]

Manuscript submitted October 16, 2018; revised manuscript received December 5, 2018. Published December 19, 2018. *This paper is part of the JES Focus Issue of Selected Papers from IMLB 2018.*

Lithium-ion batteries have been widely used in electronic devices and transportation, which are key devices for current and future society. However, lithium-ion batteries currently face safety concerns related to two critical challenges: the flammability of the liquid electrolytes and their high energy density, especially for applications in electric vehicles and energy storage systems. All-solid-state lithium batteries (ASSBs) with a sulfide-based solid electrolyte have attracted considerable attention as one of the best possible solutions due to their high energy density and their potential to be compatible with Li metal and nonflammable inorganic solid electrolytes. The challenge for ASSBs is the lithium ion path in the solid components. Not only a high lithium ion conductivity of the solid electrolyte, but also a large contact area between the solid electrolyte and the active materials are mandatory. Furthermore, sulfide-based solid electrolytes have unique mechanical properties such that the grain boundary resistance is small. The sulfide-based solid electrolytes, such as $Li_{10}GeP_2S_{12}$, $Li_7P_3S_{11}$, and Li_2S-P_2S_5 glasses, are promising solid electrolytes for ASSBs with high lithium ion conductivity (10^{-2} – 10^{-4} S cm^{-1}).[1,2] Among them, Li_6PS_5X (X = Cl, Br, I) with an argyrodite structure exhibits a rather high lithium ion conductivity of 10^{-2} – 10^{-3} S cm^{-1} at room temperature. For these reasons, favorable interfaces between active material and solid electrolyte are easily formed by preparing composite cathode of ASSBs and moderate to apply for the composite cathode. Nonetheless, it is difficult to prepare a cathode composite with a large contact area between the solid electrolyte and the active materials by a solid process of mixing the two powders. In contrast, a solution process has the advantage of preparing the composite cathode by forming the solid electrolyte layer on active materials with a precursor solution of solid electrolyte because the starting materials are dissolved in a solvent and subsequently precipitated, and consequently the particle size of the solid electrolyte is smaller than that of the mechanically milled solid electrolyte. Thus, a large contact area between the solid-solid particles as well as a reduction of the thickness of the electrolyte layer can be achieved.[3,4] Significantly, the electrolyte coating formed as a solid electrolyte layer on the active material by the solution process can bring a large contact area, although the weight ratio of the active material in the composite cathode increases so that an increase of capacity can be expected from the solution process. For this reason, the synthesis of Li_6PS_5Br and Li_6PS_5Cl with high lithium ion conductivity, which is of particular interest for a solution process using ethanol, has been recently reported as an alternative method to mechanical milling.[5,6] Li_6PS_5Cl is of particular interest due to its extraordinarily high conductivity in the crystalline phase.

The solution process includes three steps. First, the solid electrolyte is synthesized by the mechanical milling method using a planetary ball mill apparatus. Second, the synthesized solid electrolyte is dissolved in ethanol to produce the precursor solution. Finally, the precursor solution is heat treated and solid electrolyte is precipitated. The mechanical milling method using a planetary ball mill apparatus often produces only gram-scale powders and takes long times, such that large-scale synthesis remains challenging. This difference is illustrated by the schematic diagram shown in Figure 1.

Recently, solid electrolytes have been synthesized without a mechanical milling process in order to overcome these problems. β-Li_3PS_4 was synthesized by reacting Li_2S and P_2S_5 in tetrahydrofuran and then treating with heat. Some of the authors have reported $Li_7P_3S_{11}$ was prepared by stirring Li_2S and P_2S_5 in 1,2-dimethoxyethane or acetonitrile. The $Li_7P_3S_{11}$ had a lithium ion conductivity of 9.7×10^{-4} S cm^{-1}. The liquid phase process has proven to be an effective method for synthesizing micro- to nano-particle solid electrolyte with controllable particle size and morphology.[7] The liquid phase process has great flexibility and control in terms of material preparation. For example, composites of solid electrolyte and active materials or solid electrolyte and conductive carbon can be obtained directly from the liquid phase process.[8,9] Unfortunately, reported ionic conductivities of solid electrolytes using the liquid process are lower than those obtained by mechanical milling or solid-state methods.[5,8,10] Additionally, there are no studies related to the liquid phase process for the use of argyrodite-type Li_6PS_5Cl without a mechanical milling process.

In this study, rod-like Li_6PS_5Cl was, for the first time, prepared as a solid electrolyte using the liquid phase process with just two steps, and excluded the mechanical milling process.[11] Importantly, we developed Li_6PS_5Cl with an argyrodite-type structure by directly synthesizing it in a liquid phase process using the only stirring, yielding a material with a high ionic conductivity of 1.1×10^{-3} S cm^{-1} and a rod-like morphology with dimensions of 20–30 μm in length and 2–3 μm in

[z]E-mail: dwshin@hanyang.ac.kr

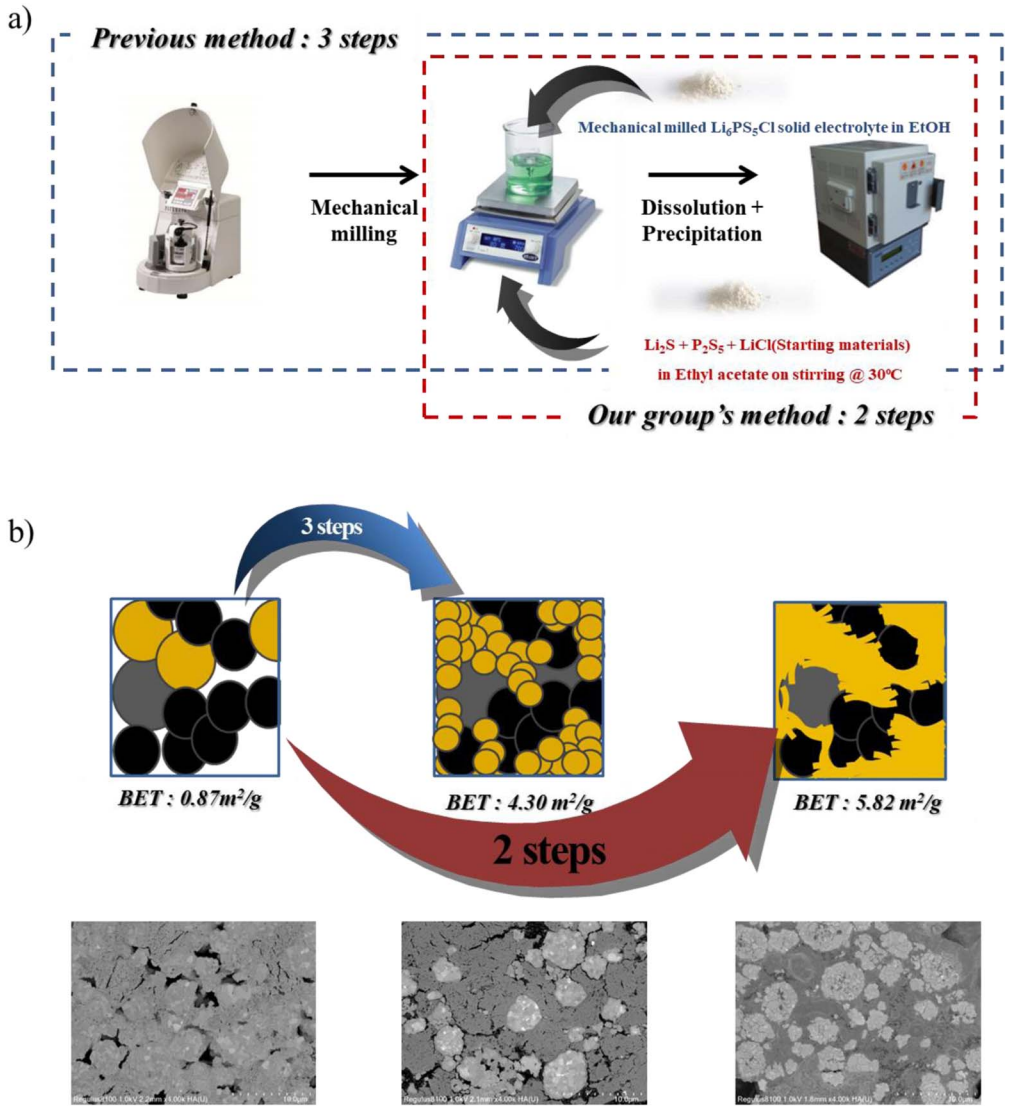

Figure 1. a) Previous method: solution process to pulverize the mechanically milled solid electrolytes, add them to the ethanol solvent; our group's method: liquid phase process to put starting materials into the ethyl acetate solvent directly. b) Differences of microstructures and specific surface area between the solid electrolytes obtained by the previous method and our group's method.

width. Reducing the solid electrolyte particle size could significantly enhance the electrochemical properties of all-solid-state batteries because the contact area between the solid electrolyte and the active materials in the composite cathode and their packing density could be increased. This method has the advantage of simple experimental manipulation, fabrication of fine solid electrolyte, and morphological control provided by the types of solvents used. The sheet-type composite cathode, composed of $LiCo_{0.6}Ni_{0.2}Mn_{0.2}O_2$ powders, solid electrolyte obtained by the liquid phase process, conducting additives, and binder as dispersant, was fabricated and evaluated as a cathode material in ASSBs in terms of its charge-discharge characteristics. We compared the above solid electrolyte with Li_6PS_5Cl obtained by mechanical milling but not the three-steps, because the Li_6PS_5Cl solid electrolyte obtained by the three-steps method had a lower ionic conductivity due to the reaction between the solid electrolyte and ethanol solvent, such that only the effect of the increased contact area of the morphology of the solid electrolyte could be differentiated.

Experimental

The solid electrolyte of Li_6PS_5Cl (Sample 1) was prepared in two steps. First, the starting materials of Li_6PS_5Cl were stirred into ethyl acetate (EA). All the synthesis processes and characterizations except for heat-treatment were performed under a dry Ar atmosphere. Reagent-grade Li_2S (Alfa Aesar, 99.9%) and LiCl (Aldrich, 99.9%) were put into the EA solvent and mixed with stirring for 1 h in order to preferentially dissolve and react due to their low solubilities. Subsequently, P_2S_5 (Aldrich, 99%) was put into the solution with stirring for 23 h at 280 rpm, where the molar ratio of Li_2S:P_2S_5:LiCl was 5:1:2. The concentration of the Li_6PS_5Cl solution was 0.06M. Second, in order to completely dry the EA from the precipitated solid electrolyte, the solution was dried at 30°C for 12 h under vacuum and then heated at a rate of 5°C min^{-1} to a final temperature of 550°C for 5 h.

To distinguish and differentiate the effects of particle size and morphology, a comparison sample of the solid electrolyte of Li_6PS_5Cl (Sample 2) was synthesized using a conventional mechanical milling method.[12] First, reagent-grade Li_2S (Alfa Aesar, 99.9%) and LiCl (Aldrich, 99.9%) were weighed and mixed at a molar ratio of 5:1:2, and the mixture was transferred to an alumina pot (volume of 100 mL) with 12 zirconia balls (10 mm in diameter) in heptane (Aldrich, anhydrous, 99%). Second, mechanical milling was carried out at 520 rpm for 45 h using a planetary ball mill apparatus (Fritsch, Pulverisette 7). Third, after removing the solvent (heptane) at 120°C for 3h, the obtained

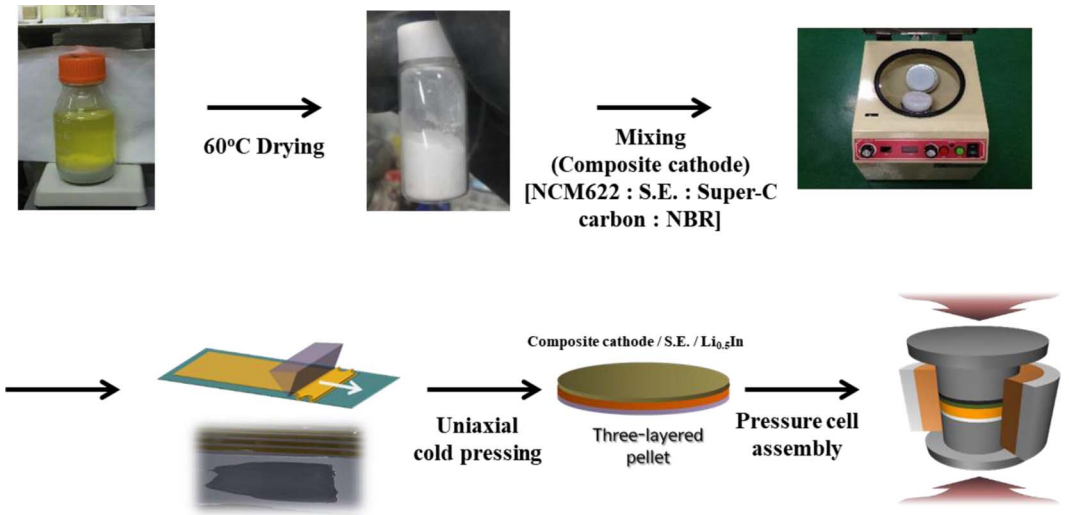

Figure 2. Fabrication method of sheet-type composite cathode used for the Li_6PS_5Cl solid electrolyte obtained by the liquid phase process.

material was heated at a rate of 5°C min^{-1} to a final temperature of 550°C for 5 h.

In order to examine the crystalline structure of both samples, X-ray diffraction (XRD) patterns of the samples were obtained with an X-ray diffractometer (Rigaku, Ultima IV) with Cu-Ka radiation (λ = 1.542 Å) at room temperature. To avoid air exposure, the samples were sealed in an airtight container covered with a polyimide thin film and mounted on the X-ray diffractometer. The Raman spectrum was measured using a Raman spectrometer (Horiba Jobin Yvon, LabRam Aramis) equipped with a 514 nm wavelength argon ion laser. The samples were pelletized with a uniaxial press under 135 MPa with an 8 mm diameter and packed into a small quartz box. The Raman spectra were measured by focusing the microscope on the surface of the sample through the quartz glass.

Ionic conductivities of the samples were measured using an electrochemical impedance analyzer (Wonatech, SP5) in the frequency range of 0.1 Hz–1 MHz. The samples were pelletized under a pressure of 140 MPa with a uniaxial press, producing pellets of 13 mm diameter and a thickness of ~1 mm. The prepared pellets were placed in a mold made from polyether ether ketone with two stainless steel rods used as blocking electrodes.

The morphology of the solid electrolytes and the microstructure of the composite cathodes were observed using a field emission scanning electron microscope (FE-SEM, S-4800, Hitachi, Japan). Cross-sectional surfaces of the composite cathodes were prepared by polishing at 6 kV for 3 h with an Ar ion beam (FE-SEM, Regulus 8100, Hitachi, Japan). The composite cathode slurry was prepared by mixing $LiNbO_3$-coated $LiNi_{0.6}Co_{0.2}Mn_{0.2}O_2$, the solid electrolytes prepared with EA and ethanol solvent, respectively, Super-P carbon (TIMCAL), and nitrile rubber in xylene with mortar and pestle at a weight ratio of 68:29:1.5:1.5. The slurries were then coated on Al foil using the doctor blade technique. The layers were dried at room temperature for 1 h and subsequently at 120°C for 2 h under vacuum. The thickness of the composite cathode sheet was 91 μm. It is thin enough to have reaction channels of the composite cathode thick film and enough to the amount of conductive additive which makes electron pathways.[13] The total surface area (Brunauer-Emmett-Teller (BET)) of the solid electrolytes were analyzed on a Micromeritics 3Flex installed at the Hanyang LINC+ Analytical Equipment Center (Seoul) to confirm the morphology of the solid electrolytes.

For the cell assembly, the composite cathode layers and Li_6PS_5Cl solid electrolyte (150 mg) were then pelletized with a uniaxial press at a pressure of 135 MPa (13 mm diameter) for 1 min, and subsequently, $Li_{0.5}In$ powders as a negative electrode were pelletized onto the opposite side of the composite cathode under 370 MPa pressure for 5 min. The $Li_{0.5}In$ powders were prepared by mixing Li (FMC Lithium Corp.) and In (99%, Sigma-Aldrich) powders. The obtained three-layer pellet was fabricated into a mold-type cell and the cell performance was investigated at room temperature using a charge-discharge measurement device (TOSCAT-3100, Toyo System, Japan) under variable C-rates. (A series of experiments are illustrated in Figure 2). Electrochemical impedance spectroscopy measurements of the prepared cells were performed using an impedance analyzer (Wonatech, SP5) in the frequency range from 0.1 Hz to 1 MHz after charging to 3.68 V after 1 charge. Galvanostatic intermittent titration technique (GITT) measurements were carried out with a pulse current of 0.1C for 10 min and rested for 30 min after 5 cycles (100% state of charge). The surface coverage of the solid electrolyte on the active material (NCM 622) was obtained by dividing the apparent surface area of the NCM 622 particles by the contact area between the NCM 622 active materials and the solid electrolyte by the GITT measurements using the following equation.[13]

$$D = \frac{4}{\pi\tau}\left(\frac{m_{NCM}V_M}{M_{NCM}S}\right)^2\left(\frac{\Delta E_s}{\Delta E_t}\right)^2 \quad [1]$$

Where D: chemical diffusion coefficient of NCM622, S: contact area between electrolyte and active materials, τ: pulse duration (600s), ΔE_s: steady-state voltage change, ΔE_t: transient voltage change, M_{ncm}: molecular weight of the host, $Ni_{0.6}Co_{0.2}Mn_{0.2}O_2$ (90.13g mol^{-1}), m_{ncm}: mass of the host in the sample (varied depending on the mass loading), V_m: molar volume of the sample (the value used was for $LiNi_{1/3}Co_{1/3}Mn_{1/3}O_2$, 20.29 cm^3 mol^{-1}).[14]

The chemical diffusion coefficient (D) of 1.72 × 10^{-11} cm^2 s^{-1} for NCM622.[13] The surface coverage values were obtained by comparing the specific surface area measured by the BET and the contact area of active materials with solid electrolytes obtained by the above mentioned GITT analysis.

Results and Discussion

The liquid phase process of the Li_2S, P_2S_5, and LiCl in EA progressed through various stages, including green and yellow transparent solutions, and resulted in the formation of a white suspension. The addition of a polar solvent resulted in the dissolution of white powders to form ion species,[11] changing the color of the solution. These results suggest the liquid phase process is a wet chemical reaction, having a complex chemistry that remains to be understood. We expect the mechanism could permit the functional groups to interact with the starting materials as recent reports suggest that an interaction between Li^+ and the lone pair of electrons on the oxygen atom in the C=O

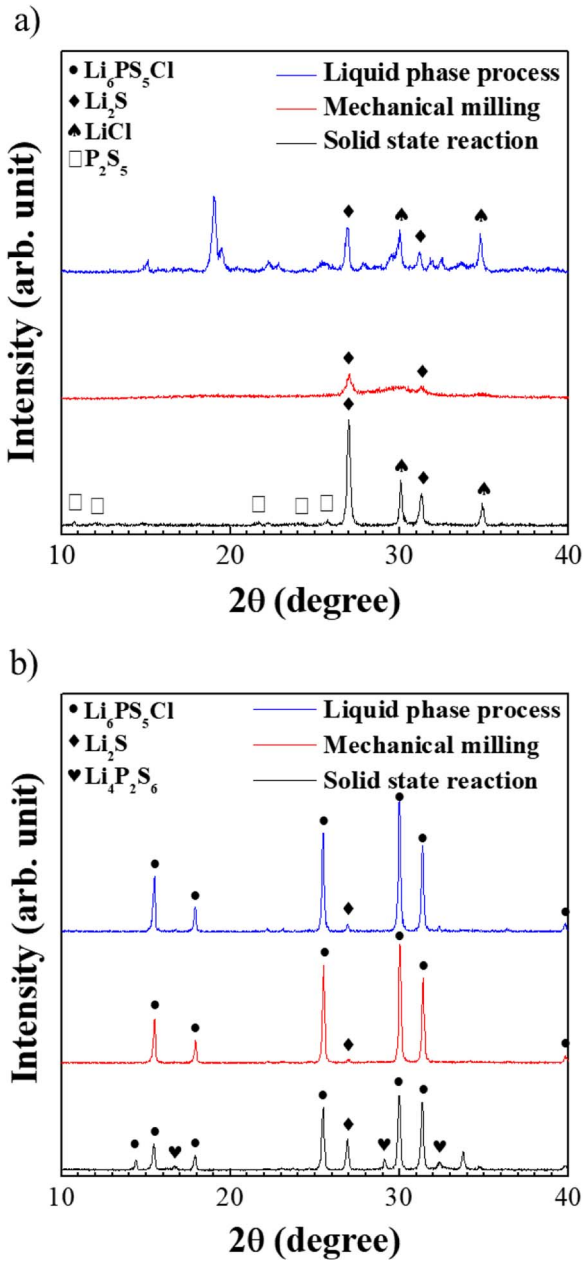

Figure 3. XRD patterns of Li_6PS_5Cl solid electrolyte obtained by the solid-state reaction, mechanical milling, and the liquid phase process. a) Before heat-treatment. b) After heat-treatment.

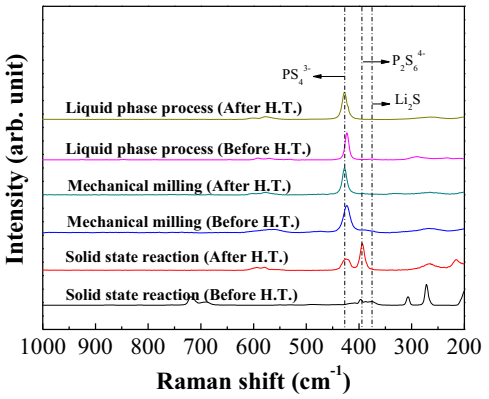

Figure 4. Raman spectra before heat-treatment and after heat-treatment of the Li_6PS_5Cl solid electrolytes obtained by the solid-state reaction, mechanical milling, and the liquid phase process.

ester group in EA.[10,11] In future work, we will further examine and determine the mechanism of the liquid phase process for the Li_6PS_5Cl solid electrolyte.

Figure 3 shows XRD patterns of the samples obtained by the solid-state reaction, mechanical milling, and liquid phase process. XRD of the samples was obtained from both the liquid phase process and mechanical milling after heat-treatment at 550°C for 5 h, which was enough to obtain well-crystallized Li_6PS_5Cl with the full removal of solvent.[15] The main peaks of Sample 1 were indexed as Li_6PS_5Cl, and minor peaks with 2θ around 27° from Li_2S (ICDD: 04-008-3440) were also detected, suggesting partial dissolution of the argyrodite structure as shown in Figure 3b. The other peaks of the structure of the argyrodite or the starting precursor materials could not be detected, implying that the crystallized argyrodite Li_6PS_5Cl phase formed well. The XRD results indicated that Li_6PS_5Cl crystal phase with minimum impurities, such as unreacted Li_2S, could be obtained by a dissolution and precipitation process via liquid phase synthesis and not just the solid-state reaction.[16] The reaction mechanism mentioned above for the liquid phase process for Li_6PS_5Cl is unclear at this moment. The exact mechanism of this reaction will be submitted and clarified soon. However, we presume that the remaining unrecorded peaks in the liquid phase processed sample seem to be lithium compounds like Li_3PS_4·EA with partially dissolved (and precipitated) Li_2S, LiCl that are generated by interaction between the solid electrolyte and solvent in the precursor as shown in Figure 3a.[17] The XRD patterns of the Li_6PS_5Cl solid electrolyte obtained by mechanical milling showed the argyrodite crystal phase and additional peaks attributed to the unreacted Li_2S phase as shown in Figure 3b.

To determine that the liquid phase process is a wet chemical reaction and not simply a solid-state reaction, a solid-state sample was synthesized by mixing the starting materials of Li_2S, P_2S_5, and LiCl without any organic liquids. The sample was heat-treated at 550°C for 5 h. The 2θ peaks around 15°, 18°, 25°, 30°, and 31° were related to the argyrodite phase while the intense 2θ peaks around 27° could be attributed to Li_2S, and the peaks at 25°, 30°, and 31° were related to $Li_4P_2S_6$ impurities, implying that it could not penetrate into the crystal structure and simply formed a lithium compound by heat-treatment. The $Li_4P_2S_6$ crystalline can decrease the cell performances due to its low conductivity but it should not significantly hinder the conduction of Li^+.[18] Therefore, the simple solid-state reaction is inappropriate to penetrate into the precursor well into the Li_6PS_5Cl crystal structure not to form the impurities. Before the heat-treatment, all of the starting materials were observed. On the other hand, some of the starting materials, such as Li_2S and LiCl, which are rather insoluble in the organic solvent,[19] were observed, indicating that the starting materials penetrated into the crystal structure partially or above and consequently precipitated the Li_6PS_5Cl solid electrolytes. Considering that not only the pure argyrodite structure precipitated by the mechanical milling was the same as the that of the Sample 1, but also the crystalline structure precipitated by the solid-state reacted sample was different from that of Sample 1, the liquid phase process formed the argyrodite structure penetrated by starting materials via dissolution and precipitation and subsequent heat-treatment.

The Raman spectra (Figure 4) show the argyrodite Li_6PS_5Cl structure of the solid-state reaction via the heat-treatment, mechanical milling, and liquid phase process. The solid-state-reacted sample showed bands around 420 cm^{-1} and 386 cm^{-1} associated with the PS_4^{3-} and $P_2S_6^{4-}$ groups, respectively, which exist as impurities formed by heat-treatment. Before the heat-treatment, peaks relating to the starting materials,[20] such as Li_2S and P_2S_5 peaks around 190 cm^{-1}, 263 cm^{-1}, 305 cm^{-1}, 686 cm^{-1}, and 715 cm^{-1}, remain without any units of the argyrodite structures, implying that the precursors could not penetrate into the crystalline structure. The LiCl peak was not observed because of the symmetry properties, and most and in

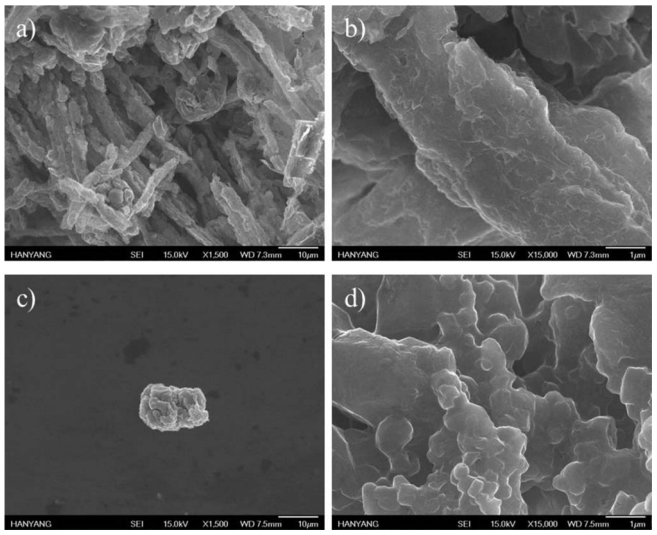

Figure 5. Morphologies of Li_6PS_5Cl solid electrolytes prepared by a), b) the liquid phase process and c), d) mechanical milling.

some cases all the fundamental modes of vibration are inactive in the Raman effect.[21] This implied that it was difficult for the starting materials with the simple heat-treatment to completely penetrate into the Li_6PS_5Cl crystal structure. On the other hand, Samples 1 and 2 showed a network of isolated PS_4^{3-} units making hexagonal cages, which were connected to each other by an interstitial site around the halide ions,[11,15] indicated by the peak around 415 cm^{-1} without any other impurity peaks. PS_4^{3-} units of the argyrodite structure were formed before the heat-treatment, displaying none of the peaks from the starting materials that were observed in the solid-state reacted sample. Thus, from these results it could be concluded that the process of dissolution-precipitation had no negative effect on forming the structure of the argyrodite-type Li_6PS_5Cl like Sample 2 obtained by the mechanical milling method, and that the chemical reaction between the solid electrolyte and the solvent was already complete before the heat-treatment. All of the results of the Raman spectroscopy agreed with the results observed in the XRD patterns.

The morphologies of the Li_6PS_5Cl solid electrolyte via the liquid phase process and mechanical milling method are presented in Figure 5. The particle of Sample 1 was about 20–30 μm in length and 2–3 μm in width, showing the morphology was a rod-like solid electrolyte. On the other hand, an uncertain morphology with dimensions of 20 – 30 μm was formed by the mechanical milling process. We expected different morphologies of the solid electrolytes when different solvents were used, considering that the Li_6PS_5Cl solid electrolyte is precipitated via interaction between the starting materials and the solvent as a reaction medium.[22] To observe the particle size of the samples, the particle size distribution was measured via laser light scattering. Sample 1 showed a submicron-scale powder with a particle sized in the range of about 12 μm, while the average particle size of Sample 2 was 22 μm. Although the both samples were not much difference in the particle size, the rod-like morphology (5.82 g cm^3) exhibited a higher specific surface area than the uncertain morphology (0.87 g cm^3). This means that the solid electrolyte could contact more active materials and endow a homogeneous distribution of the solid electrolytes and active materials into the composite cathode.[4]

Figure 6 shows typical Nyquist plots for Samples 1 and 2. Both samples displayed only blocking electrode behavior, so it was difficult to separate the contributions due to resistance from the bulk materials and those from the grain-boundaries. However, the total resistance R (Resistances of the bulk materials and grain-boundaries) can be read directly from the x-intercept of the semicircle in Figure 6a, yielding 63 Ω and 55 Ω for Samples 1 and 2, respectively.[23] The semicircle is due to increasement of the grain-boundary resistance, which

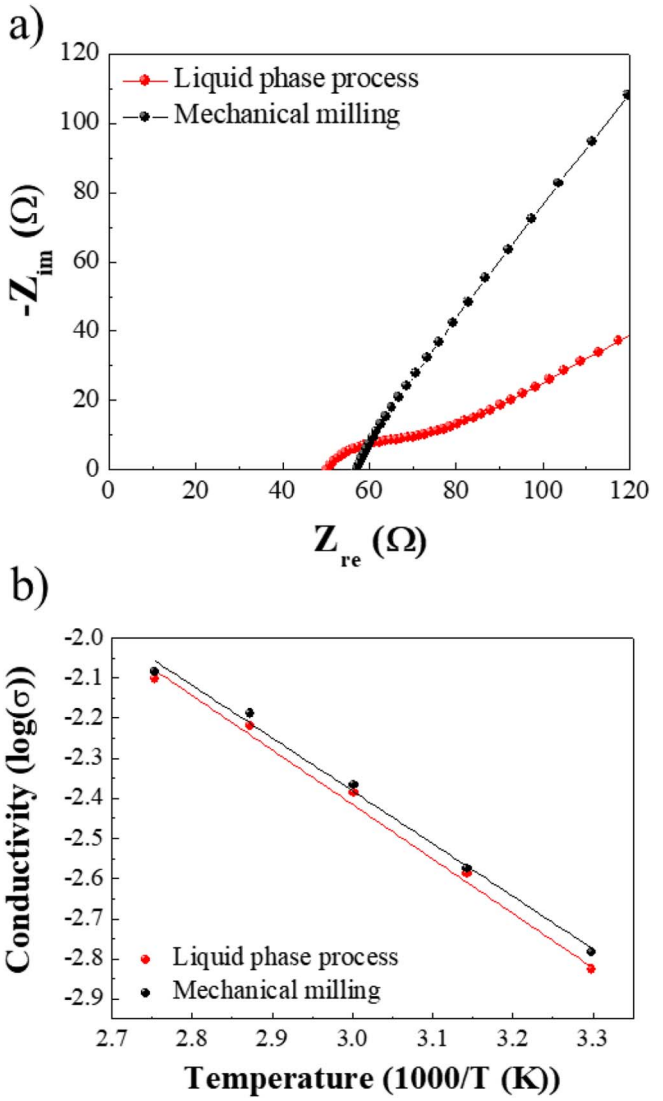

Figure 6. Plots of Li_6PS_5Cl solid electrolytes prepared by liquid phase process (closed red circles) and mechanical milling (closed black circles). a) Nyquist plots. b) Arrhenius plots.

some less-conductive organic components may remain on the surface of the solid electrolyte obtained from the polar solvent (EA).[24] The lithium ion conductivity could then be calculated from the equation[3] using the pellet area A = 1.327 cm^2 (D = 1.3 cm) and thickness (l = 0.1 cm), producing a room temperature ionic conductivity of 1.1 × 10^{-3} S·cm^{-1} for Sample 1 and 1.4 × 10^{-3} S·cm^{-1} for Sample 2. Furthermore, the calculated energy was calculated on the basis of the Arrhenius equation. It can be seen in Figure 6b that the total ionic conductivities showed good Arrhenius behavior in the entire temperature range with an activation energy of 26.0 kJ mol^{-1} for Sample 1 and 25.2 kJ mol^{-1} for Sample 2. Both samples showed a reasonably high conductivity, with a lower value in Sample 1, likely due to unreacted Li_2S starting material and possibly residual solvent impurities (see Figure 1).[5] Despite the presence of the grain boundary resistance, the relatively small loss of the ionic conductivity seemed to be due to the improvement of the crystallinity and the better densification of the pellet with higher specific surface area, even though it was from the liquid phase process.[25] The smaller the particle size of the electrolyte, the more the ionic conductivity was increased because of the increased concentration of the mobile species at the solid-solid interfaces between the electrolytes.[26] The conductivity of the Li_6PS_5Cl prepared by the liquid phase process via stirring was the highest among the solid

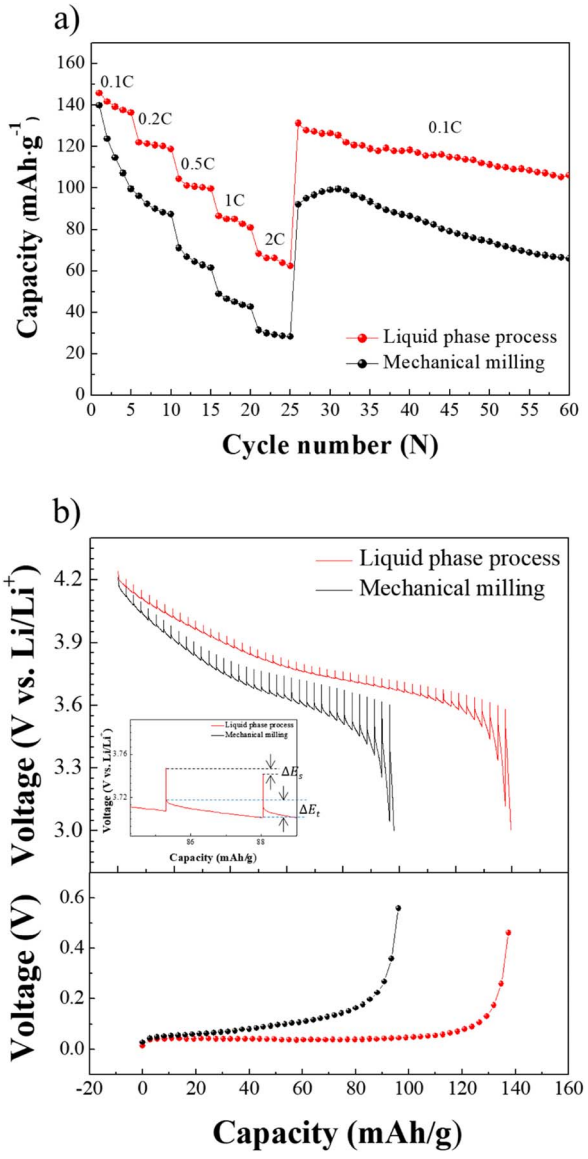

Figure 7. a) Rate performances and b) transient discharge voltage profile obtained from GITT measurements (0.1C after 5 cycles), in terms of discharge capacities, of the Li_6PS_5Cl solid electrolytes prepared by the liquid phase process and by mechanical milling.

electrolytes obtained by the liquid phase process from the reported articles[27] and for the first time exceeded 10^{-3} S·cm^{-1}. Therefore, the solid electrolyte from the liquid phase process, especially using EA as a solvent, is regarded as the moderate ion conductivity to apply for the ASSBs.

For these reasons, it is noteworthy that the liquid phase process for the Li_6PS_5Cl solid electrolyte is a way to yield the formation of highly conductive lithium ion argyrodite crystal phase solely from a practical and effective stirring method. In particular, this study is valuable because the previous studies have not demonstrated ionic conductivity from a liquid phase process.[27]

To investigate the effect of morphology of the solid electrolyte, galvanostatic charge-discharge cycling was performed in the potential range of 3.0−4.3 V (vs. Li/Li$^+$) at different C-rates (0.05 – 1.0C) as shown in Figure 7. Despite the slightly lower ionic conductivity in Sample 1, the much higher specific surface area of the solid electrolyte was expected to significantly improve the all-solid-state lithium battery performance. The cell of Sample 1 exhibited a capacity of 145.8 mAh·g^{-1} for the first discharge at 0.1C and its capacity of 62.2 mAh·g^{-1} after 25 cycles at 2C. Its efficiency was 42.67%, corresponding to the initial capacity, while the efficiency of the cell with Sample 2 was 20.16%, corresponding to the initial capacity. Both samples exhibited a similar initial discharge capacity of approximately 145.8 or 139.8 mAh·g^{-1}. During the first few cycles, both samples showed a relatively rapid capacity fading compared to the other cycles due to the increased interfacial resistance and initial irreversible capacity of the cells.[28] However, as the rate was increased, Sample 1 began to show better retention of its rate capability than Sample 2 for all C-rates, which was attributed to the more intimate ionic contacts between the active material and the solid electrolyte with a higher specific surface area. This conclusion is also supported by the GITT which was employed to track the polarization, and surface coverage of the solid electrolyte on the active material. Transient voltage profiles and polarization curves for NCM 622/solid electrolytes/Li-In cells are plotted in Figure 7b.[29] The whole range showed a higher polarization for Sample 1 than for Sample 2. The surface coverage of the solid electrolyte on the active material for Sample 1 obtained by GITT analysis was 38.4%[30] as shown in Table I. This value was about 2 times higher than that of Sample 2 (16.7%), which had balanced electronic and ionic conduction pathways due to the well-formed and intimate contact area between the solid electrolyte and active materials in the composite cathode. On the other hand, Sample 2 showed rapid capacity degradation during charge-discharge cycling since lots of voids increase accelerate the loss of contact, insufficient ionic contacts occur at solid electrolyte and active materials, limiting the utilization of the active materials. Despite the above issue, Sample 1 retains relatively well the contact area and helps the active materials utilize effectively during the charge-discharge cycling because of its solid electrolyte with the higher specific surface area, better densification and fluidity and softness of the dense electrolyte layer in the composite cathode.[31,32]

Electrochemical impedance spectroscopy was performed to verify the electrochemical performance and to determine the origin of the electrochemical behavior differences between the liquid phase processed and the mechanically-milled samples. Figure 8 shows the impedance plots of both samples with full charging at a 0.1C rate, and the values and electrochemical origins of the resistance of each component were separated as shown in Tables Ia, Ib. There is a corresponding resistance identified with each component of the batteries, that is the equivalent circuit: R_{ohm} is the solid electrolyte layer between the composite cathode R_c and anode R_a. In our previous work, we showed that the composite cathode could be further separated into two components: R_1, the pathway resistance between the solid-solid electrolyte in the composite cathode, and R_2, the interfacial resistance between the solid electrolyte and the NCM active material in the composite cathode R_c in the middle frequency region.[3,33] The Warburg tail at low frequency originates from Li ion diffusion in the active material.[34] Both R_{ohm} and R_a were almost the same for all samples as expected because we prepared both cells using the all the same components in the composite cathodes other than the solid electrolytes with different particle size and, especially morphology. Furthermore, the R_a is the resistance of the anode which is affected by changes in lithium ion concentration according to charging state of the cell, especially only affected during the discharge, but not charge, of the cell. This behavior has recently been attributed to a kinetic hindrance using lithium-indium alloy as anode. That is, the resistance of the anode increases mainly and significantly at low Li concentration in the alloy upon delithiation.[35,36] As the ionic conductivity of the solid electrolyte obtained by Sample 2 was higher than that of Sample 1, R_{ohm} of Sample 2 was rather smaller than that of Sample 1. However, the pathway resistance R_1 and interfacial resistance R_2 increased significantly with increasing particle size as well as reducing specific surface area of the solid electrolyte in the composite cathode, similar to the mechanically-milled Sample 2. This indicated that both the interfacial and pathway resistances have equivalent contributions for the cell performances because we prepared both cells using the all the same components in the composite cathodes other than the solid electrolytes with different particle size and, especially morphology. For

Table I. a) Resistance values and b) electrochemical origins of the all-solid-state cells using the liquid phase process and mechanical milling in a composite cathode with 0.1C after 1st cycle.

Table I(a)

Conditions	R_{ohm} (Ω)	R_c (Ω)			R_a (Ω)	Total (Ω)	Surface coverage of SEs onto active material [%]
		R_1	R_2	R_1+R_2			
Liquid phase process	60	11	16	27	13	111	38.4
Mechanical milling	55	25	34	59	13	142	16.7

Table I(b)

Process		Electrochemical origin
R_{ohm}		Ionic conduction in solid electrolyte
R_c	R_1	Li^+ ion migration through interface layer
	R_2	Charge-transfer between SE and active material
R_a		Li diffusion in Li-In
W		Solid state diffusion in active material

this reason, the R_1 and R_2 resistances are expected to increase more significantly at high rates in Sample 2 because the bigger size, unfavorable contact area, and uncertain morphology with lower specific surface area of the solid electrolyte will restrict the flow of the lithium ion while creating volume changes. Finally, as the resistance of the cell increased, the discharge capacity decreased, resulting in capacity degradation. From these results, it is clear that the particle size and morphologies of the solid electrolyte in the composite cathode are important regarding the rate performance of all-solid-state batteries, especially the aspect of the contact area between the solid electrolyte and active material in the all-solid-state composite cathode.

Based on these results, we observed the effect of morphology for the solid electrolyte on the lithium ion migration through the composite cathode. Figure 9 shows microstructures of the composite cathode with the solid electrolyte particles having high specific surface area. Sample 1 had rod-like solid electrolytes with a BET surface area of 5.87 $m^2\ g^{-1}$ in the composite cathode such that significantly sufficient paths for lithium ion conduction could be formed (see Figure 1). With over 6 times the specific surface area, Sample 1 would provide more interfacial contact with the active material in the composite cathode. Solid electrolytes with smaller particle size or high specific surface area like Sample 1 make a highly dense electrode layer and a solid electrolyte layer can be achieved with few voids, as shown in Figure 9b. The solid electrolytes were distributed by filling the spaces between the NCM active material with few voids, exhibiting a smooth and flat surface as shown in Figure 9a. Furthermore, size reduction of the solid electrolyte would improve the homogeneous distribution of the solid electrolyte in the active materials matrix,[4] thereby facilitating excellent ionic conduction pathways in the composite cathode. On the other hand, if an unfavorable contact area between the mechanically milled solid electrolytes were formed, it would result in disconnected lithium ion pathways and electrolyte-active material interfaces because of the multitude of voids and the significantly lower discharge capacities as shown in Figures 9c, 9d. These comparisons highlight that both the lithium ion pathway and the electrolyte-active material interface have a crucial influence on the rate performance for all-solid-state lithium batteries. NCM active materials restrict the ionic conduction pathway and isolate solid electrolyte particles because of the large number of voids on the composite cathode surface. The continuous lithium ion and electron conducting pathways were rarely formed between the solid-solid interfaces in the composite cathodes prepared by mixing the solid electrolyte powders with the solid

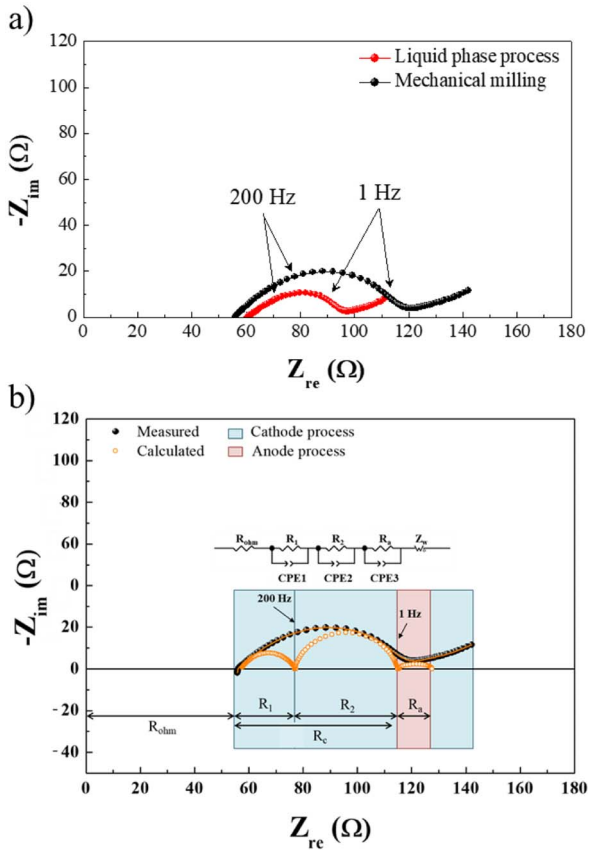

Figure 8. Electrochemical impedance spectra of Li_6PS_5Cl solid electrolytes prepared by the liquid phase process and mechanical milling after 1 charge.

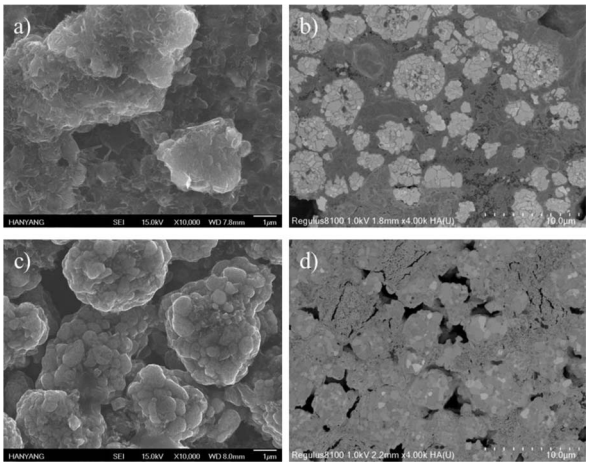

Figure 9. Microstructures of a) surface, b) cross-section on the composite cathode applied for a), b) the liquid phase processed Li_6PS_5Cl solid electrolytes and c) surface, d) cross-section on the composite cathode applied for the mechanical milled Li_6PS_5Cl solid electrolytes.

active materials and conductive additives due to the lack of fluidity of the solid electrolyte powders in the all-solid-state cells, while effective electrode (solid) – electrolyte (liquid) interfaces were easily formed by immersing the electrodes in liquid electrolyte in cells using organic liquid electrolytes. Therefore, we purposely ensured the microstructure had a large contact area between the active material and the solid electrolyte in the all-solid-state composite cathode. We are sure that this study has devised a way to increase the contact area between the active materials and solid electrolytes in the composite cathode in addition to the solid electrolyte coated on active materials via the liquid phase process, especially for the solid electrolyte with the higher specific surface area like the rod-like morphology (see Figure 1).

Conclusions

Argyrodite-type Li_6PS_5Cl solid electrolytes were, for the first time, prepared by a liquid-phase process with EA as a solvent and subsequent heat-treatment at 550°C without any mechanical milling process. The preparation conditions, such as kind of the solvent, dissolution time, drying temperature, and fabrication method, were examined, resulting in a Li_6PS_5Cl solid electrolyte with a relatively high lithium-ion conductivity of 1.1×10^{-3} S·cm^{-1} at room temperature, which was comparable to the mechanical milling process. This process has the advantages of simple synthesis, fabrication of fine powders without additional pulverization such as in the mechanical milling process, and large-scale production. The cell using the composite cathode prepared by this process exhibited a capacity of 145 mAh·g^{-1} for the first discharge at 0.1C and a capacity of 62 mAh·g^{-1} after 25 cycles at 2C. Its efficiency was 42.67%, corresponding to the initial capacity, while the efficiency of the cell prepared by mechanical milling was 20.16%, corresponding to the initial capacity. The liquid phase process formed favorable lithium ionic conduction paths as well as solid-solid interfaces between the active material and solid electrolyte particles with high specific surface area due to the rod-like morphology of the electrolytes. We believe that the dissolution-precipitation of argyrodite-type sulfide-based solid electrolytes with EA is a promising way to generate high cell performance.

Acknowledgments

This work was supported by an industrial–academic collaboration program funded by the Hyundai Motor Company.

ORCID

Dongwook Shin https://orcid.org/0000-0002-8829-9638

References

1. Y. Kato, K. Kawamoto, R. Kanno, and M. Hirayama, *Electrochemistry*, **80**, 749 (2012).
2. H. Yamane, M. Shibata, Y. Shimane, T. Junke, Y. Seino, S. Adams, K. Minami, A. Hayashi, and M. Tatsumisago, *Solid State Ionics*, **178**, 1163 (2007).
3. S. Choi, S. Lee, J. Park, W. T. Nichols, and D. Shin, *Applied Surface Science*, **444**, 10 (2018).
4. A. Sakuda, T. Takeuchi, and H. Kobayashi, *Solid State Ionics*, **285**, 112 (2016).
5. S. Yubuchi, S. Teragawa, K. Aso, K. Tadanaga, A. Hayashi, and M. Tatsumisago, *Journal of Power Sources*, **293**, 941 (2015).
6. N. C. Rosero-Navarro, A. Miura, and K. Tadanaga, *Journal of Sol-Gel Science and Technology*, (2018).
7. Y. Wang, D. Lu, M. Bowden, P. Z. El Khoury, K. S. Han, Z. D. Deng, J. Xiao, J.-G. Zhang, and J. Liu, *Chem. Mater.*, **30**, 990 (2018).
8. F. Han, J. Yue, X. Fan, T. Gao, C. Luo, Z. Ma, L. Suo, and C. Wang, *Nano Lett.*, **16**, 4521 (2016).
9. X. Yao, D. Liu, C. Wang, P. Long, G. Peng, Y. S. Hu, H. Li, L. Chen, and X. Xu, *Nano Lett.*, **16**, 7148 (2016).
10. S. Ito, M. Nakakita, Y. Aihara, T. Uehara, and N. Machida, *Journal of Power Sources*, **271**, 342 (2014).
11. N. H. H. Phuc, K. Morikawa, T. Mitsuhiro, H. Muto, and A. Matsuda, *Ionics*, **23**, 2061 (2017).
12. S. Boulineau, M. Courty, J.-M. Tarascon, and V. Viallet, *Solid State Ionics*, **221**, 1 (2012).
13. Y. J. Nam, D. Y. Oh, S. H. Jung, and Y. S. Jung, *Journal of Power Sources*, **375**, 93 (2018).
14. K. M. Shaju, G. V. Subba Rao, and B. V. R. Chowdari, *Journal of The Electrochemical Society*, **151**, A1324 (2004).
15. P. R. Rayavarapu, N. Sharma, V. K. Peterson, and S. Adams, *Journal of Solid State Electrochemistry*, **16**, 1807 (2011).
16. N. C. Rosero-Navarro, A. Miura, and K. Tadanaga, *Journal of Power Sources*, **396**, 33 (2018).
17. N. Phuc, K. Morikawa, M. Totani, H. Muto, and A. Matsuda, *Chemical synthesis of Li3PS4 precursor suspension by liquid-phase shaking*, (2015).
18. Y. Suto, Y. Fujii, A. Miura, N. C. Rosero-Navarro, M. Higuchi, and K. Tadanaga, *Journal of the Ceramic Society of Japan*, **126**, 568 (2018).
19. X. Li, C. A. Wolden, C. Ban, and Y. Yang, *ACS Appl Mater Interfaces*, **7**, 28444 (2015).
20. S. S. Berbano, I. Seo, C. M. Bischoff, K. E. Schuller, and S. W. Martin, *Journal of Non-Crystalline Solids*, **358**, 93 (2012).
21. R. S. Krishnan, in *Essays in Structural Chemistry*, A. J. Downs, D. A. Long, and L. A. K. Staveley Editors, p. 189, Springer US, Boston, MA (1971).
22. F. Vaquero, R. M. Navarro, and J. L. G. Fierro, *Applied Catalysis B: Environmental*, **203**, 753 (2017).
23. R. C. Xu, X. H. Xia, Z. J. Yao, X. L. Wang, C. D. Gu, and J. P. Tu, *Electrochimica Acta*, **219**, 235 (2016).
24. S. Yubuchi, S. Teragawa, K. Aso, K. Tadanaga, A. Hayashi, and M. Tatsumisago, *Journal of Power Sources*, **293**, 941 (2015).
25. Z. C. Liu, W. J. Fu, E. A. Payzant, X. Yu, Z. L. Wu, N. J. Dudney, J. Kiggans, K. L. Hong, A. J. Rondinone, and C. D. Liang, *J. Am. Chem. Soc.*, **135**, 975 (2013).
26. N. Sata, K. Eberman, K. Eberl, and J. Maier, *Nature*, **408**, 946 (2000).
27. K. H. Park, Q. Bai, D. H. Kim, D. Y. Oh, Y. Zhu, Y. Mo, and Y. S. Jung, *Advanced Energy Materials*, **8**, (2018).
28. A. Sakuda, A. Hayashi, and M. Tatsumisago, *Chem. Mater.*, **22**, 949 (2010).
29. Y. S. Jung, K. T. Lee, J. H. Ryu, D. Im, and S. M. Oh, *Journal of The Electrochemical Society*, **152**, A1452 (2005).
30. D. H. Kim, D. Y. Oh, K. H. Park, Y. E. Choi, Y. J. Nam, H. A. Lee, S. M. Lee, and Y. S. Jung, *Nano Lett.*, **17**, 3013 (2017).
31. R.-C. Xu, X.-H. Xia, S.-H. Li, S.-Z. Zhang, X.-L. Wang, and J.-P. Tu, *Journal of Materials Chemistry A*, **5**, 6310 (2017).
32. A. Sakuda, *Journal of the Ceramic Society of Japan*, **126**, 675 (2018).
33. S. Noh, W. T. Nichols, C. Park, and D. Shin, *Ceramics International*, **43**, 15952 (2017).
34. K. H. Park, D. Y. Oh, Y. E. Choi, Y. J. Nam, L. Han, J. Y. Kim, H. Xin, F. Lin, S. M. Oh, and Y. S. Jung, *Adv Mater*, **28**, 1874 (2016).
35. A. Sakuda, H. Kitaura, A. Hayashi, K. Tadanaga, and M. Tatsumisago, *Journal of The Electrochemical Society*, **156**, A27 (2009).
36. W. Zhang, D. A. Weber, H. Weigand, T. Arlt, I. Manke, D. Schroder, R. Koerver, T. Leichtweiss, P. Hartmann, W. G. Zeier, and J. Janek, *ACS Appl Mater Interfaces*, **9**, 17835 (2017).